

# Theory for Growth of Needle-shaped Particles in Multicomponent Systems

P.E.J. Rivera-Díaz-del-Castillo and H.K.D.H. Bhadeshia

University of Cambridge

Department of Materials Science and Metallurgy

Pembroke Street, Cambridge CB2 3QZ, U.K.

## ABSTRACT

A solution is presented for the growth of needle-shaped particles (paraboloids of revolution) in multicomponent systems that obey Henry's law. Interface kinetics and capillarity effects are incorporated, and it is demonstrated that the maximum velocity hypothesis cannot be sustained if it is assumed that there is local equilibrium at the interface. The particle is unable to grow with equilibrium for small supersaturations when capillarity effects are prominent, and for large supersaturations when the interface kinetics effect is large. A method to obtain the lengthening rate and tip radius is provided.

## Introduction

There is a variety of models dealing with the diffusion-controlled growth of needle-like particles with the idealised shape of a paraboloid of revolution. Some of the original work in this area was done by Ivanstov [1] and Horvay and Cahn [2], who presented exact solutions to the diffusion equation for an isoconcentrate boundary. Their model is expressed mathematically as:

$$\Omega = p \exp\{p\} E_1\{p\} \quad (1)$$

where  $p = v\rho/2D$  is the Péclet number,  $v$  is the lengthening rate,  $\rho$  is the radius of curvature of the tip of the paraboloid,  $D$  is the diffusion coefficient of the solute in the matrix phase,  $E_1$  the exponential integral [3] and  $\Omega$  is the dimensionless supersaturation given by

$$\Omega = \frac{\bar{c} - c^{\alpha\beta}}{c^{\beta\alpha} - c^{\alpha\beta}} \quad (2)$$

where  $\bar{c}$  is the average solute concentration in the alloy,  $c^{\alpha\beta}$  is the solute concentration of the matrix ( $\alpha$ ) in equilibrium with the precipitate ( $\beta$ ),  $c^{\beta\alpha}$  is the corresponding concentration in the precipitate in equilibrium with the matrix.

Trivedi [4,5] pointed out the non-isoconcentrate nature of the interface, and incorporated capillarity and interface kinetics effects

$$\Omega = p \exp\{p\} E_1\{p\} \left[ \underbrace{1}_a + \underbrace{\frac{v}{v_c} \Omega R_1\{p\}}_b + \underbrace{\frac{\rho_c}{\rho} \Omega R_2\{p\}}_c \right] \quad (3)$$

where  $v_c = \mu(\bar{c} - c^{\alpha\beta})$  is the velocity of a flat interface during interface-controlled growth, i.e., when almost all the free energy is dissipated in the transfer of atoms across the boundary causing the concentration difference in the matrix to vanish, and  $\mu$  is the interface kinetics coefficient. For curved interfaces, the growth rate will become zero at a curvature  $1/\rho_c$  via the Gibbs-Thomson effect [6]. The functions  $R_1 = \frac{1}{2p} N_1\{p\} - 1$  and  $R_2 = \frac{1}{4p} N_2\{p\} - 1$  have been evaluated numerically by Trivedi [4] for large supersaturations, and have recently been extended for small values of  $\Omega$  [7]; such functions account for the concentration change along the parabolic surface.

The term labelled  $a$  in equation (3) is the Ivanstov solution [1] where interface kinetics and capillarity effects are neglected; terms  $b$  and  $c$  account respectively for those effects. Equation (3) does not provide a unique answer for the growth rate  $v$ , which depends on the tip radius  $\rho$ . For solid-state transformations it is common to adopt Zener's assumption [7-10] that the radius of curvature is that which gives the maximum growth rate. This is obtained by differentiating equation (3) with respect to  $\rho$  and setting  $\partial v/\partial \rho = 0$ , which gives

$$0 = (g^*\{p\})^2 \frac{\rho_c}{\rho} \left( 2 \frac{p}{q^*} R'_1\{p\} - \frac{1}{p} R_2\{p\} + R'_2\{p\} \right) + \frac{g^*\{p\}}{p} + g^*\{p\} - 1 \quad (4)$$

where  $g^*\{p\} = p \exp\{p\} E_1\{p\}$  and

$$q^* = \frac{\mu(\bar{c} - c^{\alpha\beta})}{2D/\rho_c} \quad (5)$$

is a parameter which indicates the relative magnitudes of the interface kinetics and the diffusion effect. The values of the functions  $R'_1$ ,  $R'_2$  are given in [7]; they can be used to solve equations (3) and (4) simultaneously, to obtain a unique solution for  $v$  and  $\rho/\rho_c$  as a function of  $\Omega$ , as long as the Zener assumption is justified.

The purpose of the present work was to extend Trivedi's work on binary alloys, to cover the growth of needles in multicomponent systems. The inspiration for this comes from Coates [11-13] who treated the growth of spheres in multicomponent systems, but we shall add the effects of capillarity and interface kinetics.

## Multicomponent needle growth with an isoconcentrate boundary

With  $i = 1, 2, \dots, m$  components diffusing during growth, it becomes necessary to solve a set of diffusion equations in parabolic coordinates. Following Ivanstov, this requires

$$\Omega_i = p_i \exp\{p_i\} E_1\{p_i\} \quad (6)$$

where  $p_i = v\rho/2D_i$ ,  $D_i$  is the diffusivity of component  $i$  and

$$\Omega_i = \frac{\bar{c}_i - c_i^{\alpha\beta}}{c_i^{\beta\alpha} - c_i^{\alpha\beta}} \quad (7)$$

is the supersaturation of component  $i$ . Since  $v$  and  $\rho$  can only have single values, simultaneous solution of equation (6) for  $i = 1, 2, \dots, m$  demands

$$p_1 D_1 = p_2 D_2 = \dots = p_m D_m \quad (8)$$

Consider now a ternary system, such as a steel. The influence of a difference in the diffusivities of two components (for example carbon and a substitutional solute) can be seen by varying  $p_2$  and obtaining  $p_1 = \frac{D_2}{D_1} p_2$ , and plotting the results in the form of Coates interface–composition (IC) contours for several values of  $D_2/D_1$ . A given IC contour is the locus of all alloy compositions for which the concentration at the transformation front are defined by the same equilibrium tie–line. Such results are shown in Fig. 1. Thus, a needle–shaped particle with an isoconcentrate interface behaves much the same as a sphere [11–13] but with  $p_1, p_2$  given by the solution of equations (6,8).

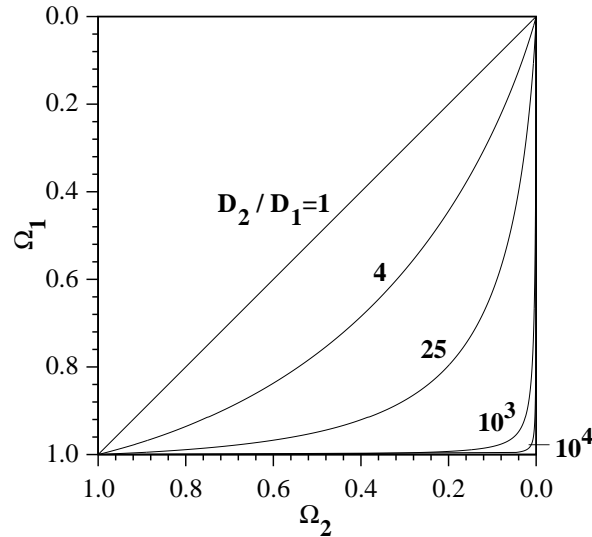


Fig. 1 Needle-shaped isoconcentrate particle IC contours for different ratios of diffusivities in a ternary system.

## Capillarity effects in multicomponent needle growth

When capillarity is taken into account during needle growth, mass balance demands for each diffusing component,

$$\Omega_i = p_i \exp\{p_i\} E_1\{p_i\} \left[ 1 + \frac{\rho_c}{\rho} \Omega_i R_2\{p_i\} \right] \quad (9)$$

for  $i = 1, 2, \dots, m$  diffusing components [4,5]. The use of the maximum velocity hypothesis gives

$$0 = (g^*\{p_i\})^2 \frac{\rho_c}{\rho} \left( -\frac{1}{p} R_2\{p_i\} + R_2'\{p_i\} \right) + \frac{g^*\{p_i\}}{p_i} + g^*\{p_i\} - 1 \quad (10)$$

for  $i = 1, 2, \dots, m$ , which gives a system of  $2m$  equations in which  $\rho$  and  $v$  are over determined. The problem will thus be inverted to seek solutions consistent with equations (8,9).

### Binary systems

First consider a particle growing at  $\rho/\rho_c = 10$  in a binary system, the corresponding values of  $p$  as a function of  $\Omega$  given by equation (9) are shown in Fig. 2a. It is seen that a minimum in  $\Omega$  is present when the critical radius  $\rho_c$  and the needle tip radius  $\rho = 10 \times \rho_c$  are maximum, as shown in Fig. 2b, where  $\rho_c$  was calculated assuming  $c^{\beta\alpha} = 0.95$ ,  $c^{\alpha\beta} = 0.05$  and  $\frac{\sigma v^\beta}{kT} = 10^{-10}$  m. As with Trivedi [4,5], the expression for  $\rho_c$  as presented below assumes that the solution obeys Henry's law, *i.e.* that the activity coefficient is constant [6, page 483]:

$$\rho_c = \frac{2c^{\alpha\beta}}{\bar{c} - c^{\alpha\beta}} \left( \frac{\sigma v^\beta}{kT} \right) \left( \frac{1}{c^{\beta\alpha} - c^{\alpha\beta}} \right) \quad (11)$$

where  $v^\beta$  is the solute atomic volume,  $k$  is the Boltzmann's constant and  $T$  the temperature. This is because the conditions at the needle tip are closest to equilibrium, as given by the phase diagram, at the largest tip radius. Note that for a given value of  $\Omega$ , there are two solutions for  $p$ , it is assumed by Trivedi [4,5] that growth occurs at the value of  $p$  that produces the maximum lengthening rate.

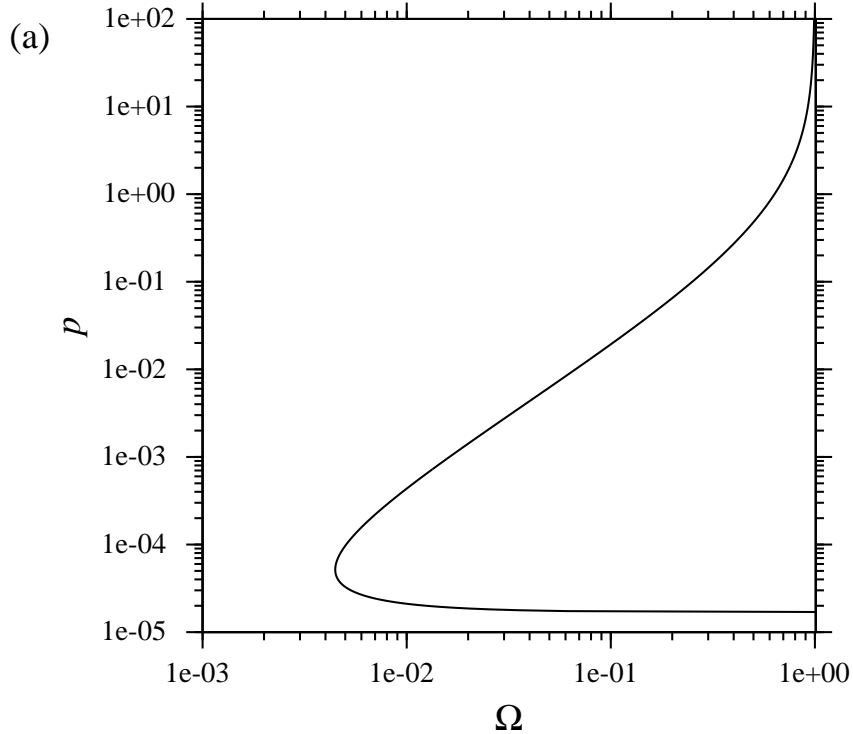
Fig. 3 shows a generic plot of equation (9), showing the variation of  $p$  with  $\Omega$  and  $\rho/\rho_c$  in a binary system. With  $\rho/\rho_c = \infty$  the plot represents the Ivanstov solution, where  $\rho$  and  $v$  cannot be defined uniquely. When  $\rho/\rho_c = 10$  capillarity plays a role in the growth process,  $\Omega$  is no longer a function that grows monotonically with  $p$ ; as  $\rho/\rho_c$  approaches to 1, capillarity becomes prominent, and the growth process has to occur at large supersaturations.

### Multicomponent systems

The Coates' concept of interface-composition contours as represented in Fig. 1 cannot be applied directly when capillarity is included in the calculations. In Fig. 1, the  $\Omega_i$  term defines

the compositions at the growing interface via equation (2), and at the same time represents the dimensionless supersaturations. Whereas  $\Omega_i$  continue to represent the supersaturations when capillarity is incorporated into the theory, the compositions at the interface are no longer  $c^{\alpha\beta}$  and  $c^{\beta\alpha}$  (equation (2)) but rather the values  $c_{\rho}^{\alpha\beta}$  and  $c_{\rho}^{\beta\alpha}$  as modified by capillarity. Therefore, the plots corresponding to Fig. 1 are best called interface–saturation (IS) contours rather than interface composition contours; as will be seen later, it is necessary to make this distinction in order to avoid confusion.

The effects of capillarity in multicomponent growth can be observed in IS contours, which in the present context illustrates the locus of points where growth under local equilibrium is possible. In the absence of capillarity, growth with local equilibrium is always possible, as illustrated in Fig. 1. Fig. 4a shows for a ternary system, the permitted values for  $\Omega_1$  and  $\Omega_2$  as  $p_2$  is varied for  $\rho/\rho_c = 6$  (see also Appendix A). Consistent with the binary case (Fig. 3), there is a minimum value of  $\Omega_2$  for the fast diffuser; larger values of  $\Omega_1$  are required when  $D_2/D_1$  is increased, because as the slow diffuser requires more driving force to keep pace with the fast diffuser. As capillarity is increased, less energy is available for diffusional growth, demanding larger supersaturations as shown in Fig. 4b for  $\rho/\rho_c = 2$ ; this effect is reduced for larger values of  $\rho/\rho_c$  (Fig. 4c).



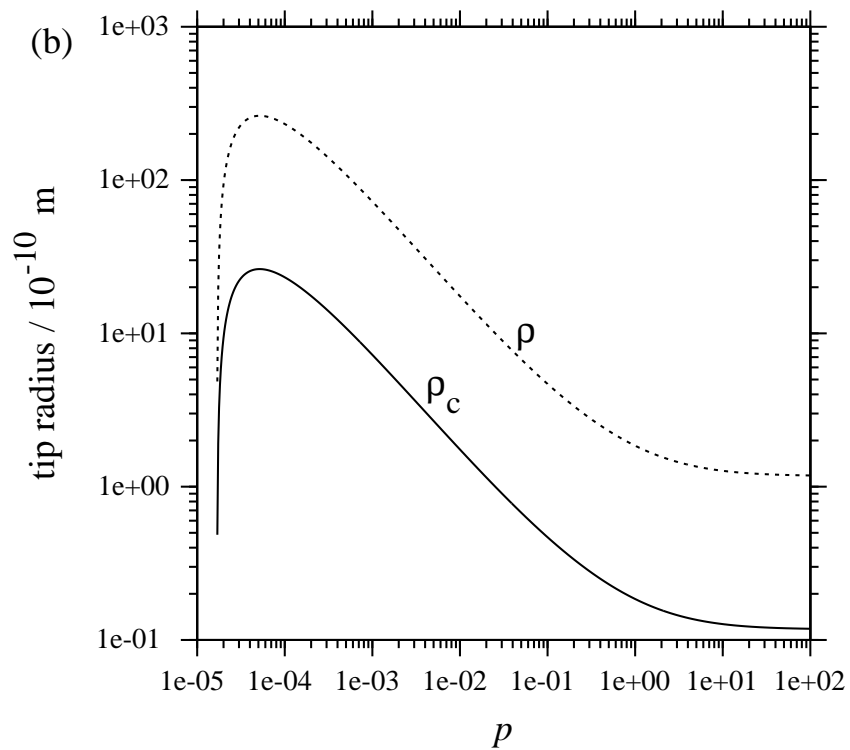


Fig. 2 Variation of (a) supersaturation and (b) critical and needle tip radius with  $p$  for  $\rho/\rho_c = 10$ .

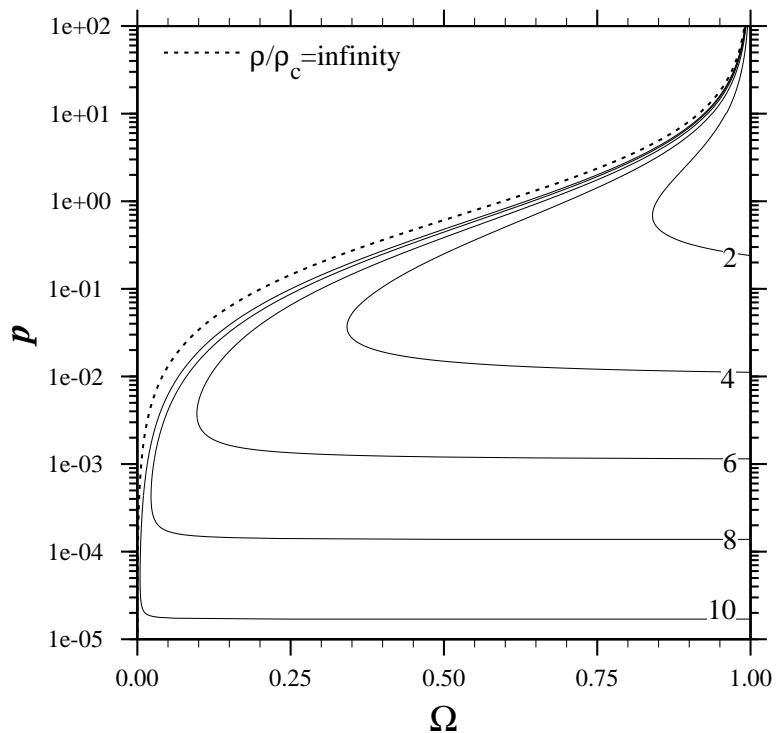


Fig. 3 Supersaturation as a function of the Péclet number and tip radius ratio.

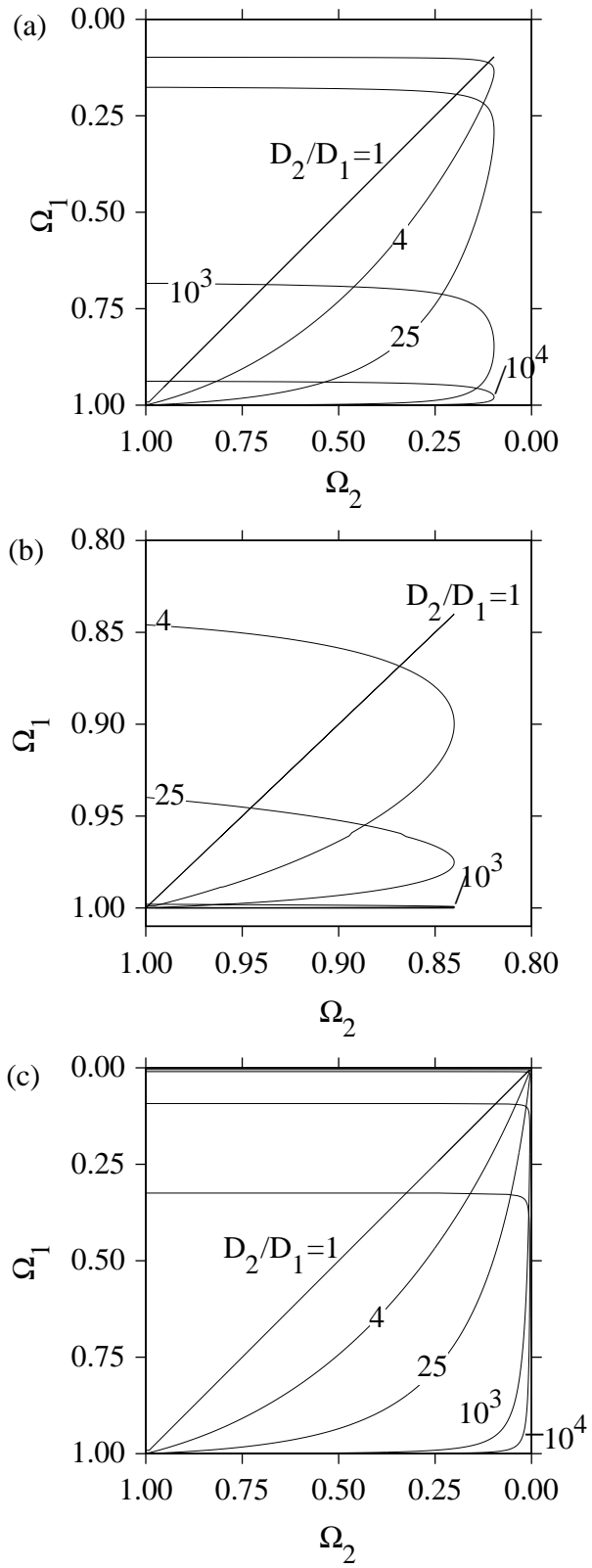


Fig. 4 IS contours in a ternary system for  $\rho/\rho_c =$  (a) 6, (b) 2, (c) 10. Note that the scale in Fig. 4b is different from 4a and 4c.

To find a solution to equations (8,9), consider an alloy of composition  $\bar{c}_i$ . In a multicomponent system, the critical radius can be calculated from the classical theory [6, page 483] as

$$\rho_c = \frac{2c_i^{\alpha\beta}}{\bar{c}_i - c_i^{\alpha\beta}} \left( \frac{\sigma v_i^\beta}{kT} \right) \left( \frac{1}{c_i^{\beta\alpha} - c_i^{\alpha\beta}} \right) \quad (12)$$

which requires that

$$\frac{c_1^{\alpha\beta}}{\bar{c}_1 - c_1^{\alpha\beta}} \frac{v_1^\beta}{c_1^{\beta\alpha} - c_1^{\alpha\beta}} = \frac{c_2^{\alpha\beta}}{\bar{c}_2 - c_2^{\alpha\beta}} \frac{v_2^\beta}{c_2^{\beta\alpha} - c_2^{\alpha\beta}} = \dots = \frac{c_m^{\alpha\beta}}{\bar{c}_m - c_m^{\alpha\beta}} \frac{v_m^\beta}{c_m^{\beta\alpha} - c_m^{\alpha\beta}} \quad (13)$$

for  $i = 1, 2, \dots, m$  components, where  $v_i^\beta$  is the atomic volume of  $i$ . Once a tie-line that satisfies equation (13) is found, the value of  $\rho_c$  can be obtained.

Consider a ternary system, choosing the appropriate equilibrium tie-line that satisfies equation (13), the values of  $c_1^{\alpha\beta}$ ,  $c_1^{\beta\alpha}$ ,  $c_2^{\alpha\beta}$ ,  $c_2^{\beta\alpha}$  can be obtained, and thus  $\Omega_1$  and  $\Omega_2$  and  $\rho_c$  calculated. Provided that the value of the diffusion coefficients of the two solutes is known,  $D_2/D_1$  can be calculated. Then the value of  $\rho/\rho_c$  can be varied until an IS contour intersects the point  $\Omega_1, \Omega_2$ . This procedure is shown in Fig. 5 for  $D_2/D_1 = 10^3$ , where the point  $\Omega_1 = 0.1$ ,  $\Omega_2 = 0.05$  is intersected only by the IS contour produced with  $\rho/\rho_c = 10$ .

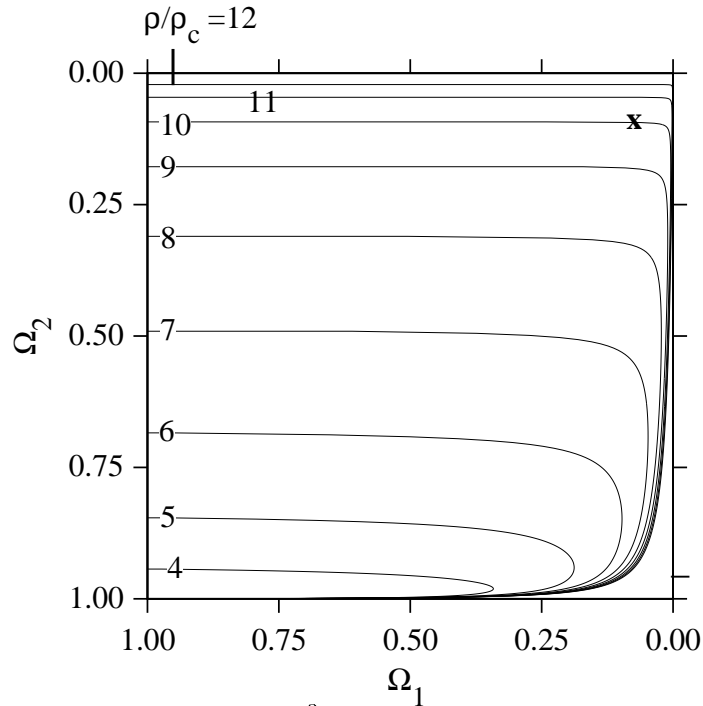


Fig. 5 IS contours for  $D_2/D_1 = 10^3$  as a function of  $\rho/\rho_c$ .



For any set of supersaturations  $\Omega_1, \Omega_2$ , there is only one possible IS contour that can be intersected (Fig. 5), implying that the value of  $\rho/\rho_c$  is unique. Furthermore, being that each point of such IS contour is associated to a unique value of  $p_2$  and  $p_1 = \frac{D_2}{D_1}p_2$ , these are uniquely defined as well.  $\rho_c$  can be obtained from the equilibrium compositions and then the velocity is determined through  $v = 2p_1D_1/\rho = 2p_2D_2/\rho$ .

Therefore, it is seen that an important consequence is that the velocity is determined uniquely, without invoking a maximum velocity hypothesis; the presence of a third element with a different diffusivity permits a unique choice of velocity when local equilibrium is assumed.

### Interface kinetics effect in multicomponent needle growth

If it is assumed that the flux  $J_i$  of solute  $i$  across the interface is only a function of the concentrations of that solute, the velocity of a flat interface can be expressed as  $v_c = \mu_i(\bar{c}_i - c_i^{\alpha\beta})$  for  $i = 1, 2, \dots, m$  components, where  $\mu_i$  is the interface kinetics coefficient of component  $i$ . The relative magnitudes of interface kinetics and diffusion effect are given by

$$q_i^* = \frac{\mu_i(\bar{c}_i - c_i^{\alpha\beta})}{2D_i/\rho_c} \quad (14)$$

Note that the critical velocity  $v_c$  decreases as  $\mu_i$  (or  $q_i^*$ ) decrease. In other words, the critical velocity decreases as it becomes more difficult to transfer atoms across the interface. An infinite value of  $q_i^*$  means that the free energy dissipated in interface kinetics is negligible.

Thus, equation (9) can be modified to include interface kinetics as

$$\Omega_i = g^*\{p_i\} \left[ 1 + 2\frac{\rho_c}{\rho} \frac{p_i}{q_i^*} \Omega_i R_1\{p_i\} + \frac{\rho_c}{\rho} \Omega_i R_2\{p_i\} \right] \quad (15)$$

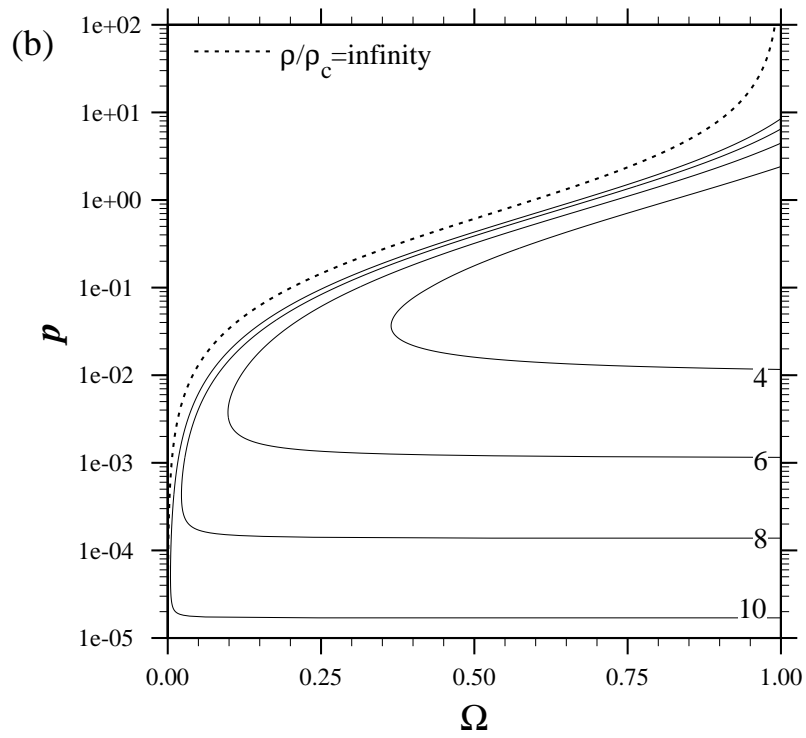
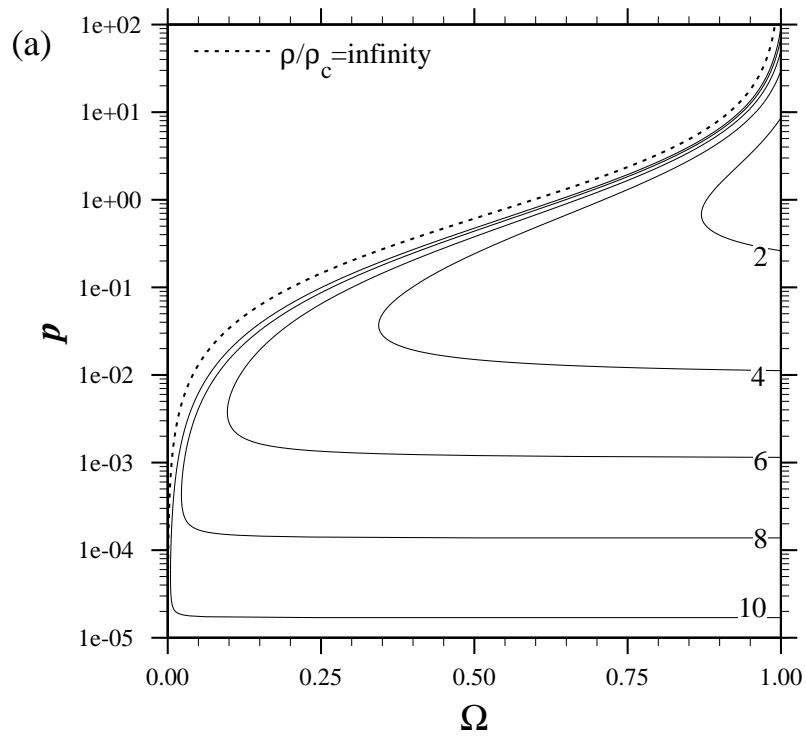
For small values of  $\rho/\rho_c$ , the solution of equation (15) for a single diffusing component is shown in Fig. 6 for the indicated values of  $q^*$ . It is to be noted that as the interface kinetics effect is increased, the permitted values of  $p$  are reduced for a given supersaturation and  $\rho/\rho_c$ . This is because at greater velocities more energy is dissipated in atom transfer across the interface, reducing the lengthening rate.

To asses the effect of multicomponent interface kinetics it is first recognised that

$$q_1^*D_1 = q_2^*D_2 = \dots = q_m^*D_m \quad (16)$$

which has to be simultaneously solved with equations (8) and (15) to satisfy mass balance at the interface.

The supersaturations that simultaneously satisfy equations (8,15,16) can be expressed as IS contours for  $m = 2$ . Fig. 7 provides an example of such contours for  $q_2^* = 0.02$ ,  $\rho/\rho_c=8$ , this shows that the addition of interface kinetics effect limits the value of  $\Omega_1$  and  $\Omega_2$  when these approach 1 due to all the energy will be depleted by this effect.



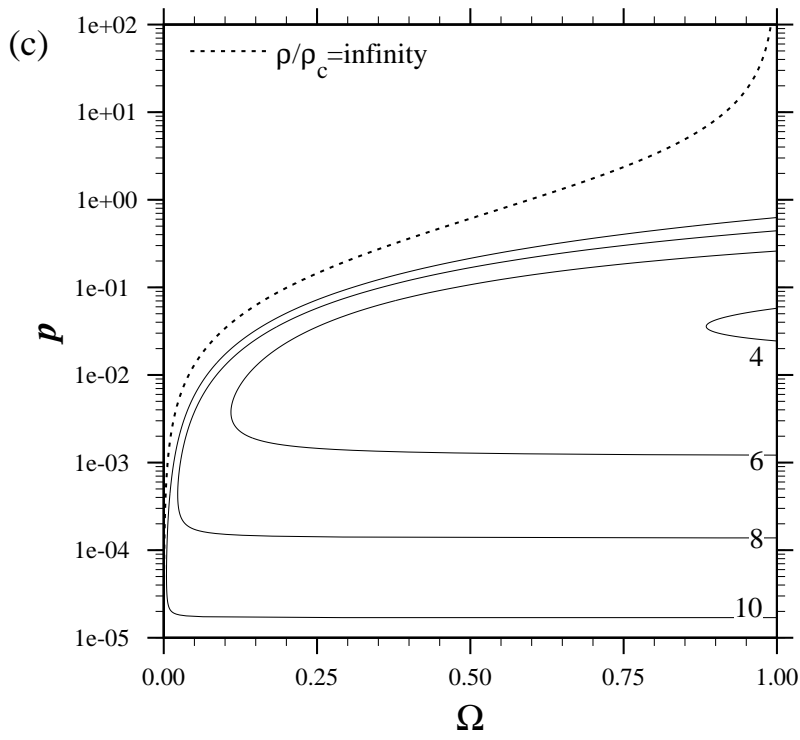


Fig. 6 Solutions for single solute for  $q^* =$  (a) 20, (b) 2, (c) 0.2

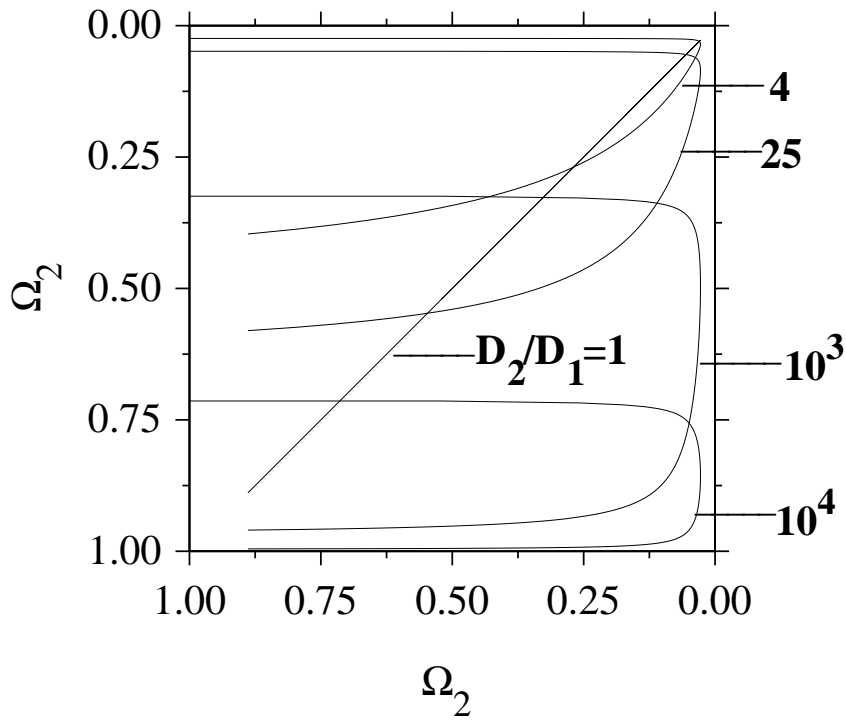


Fig. 7 IS contours for  $q^* = 0.02$  and  $\rho/\rho_c = 8$

The overall effect of interface kinetics is to reduce the particle lengthening velocity, and limit this to a maximum value as  $\Omega_i \rightarrow 1$ . The procedure to obtain the lengthening rate and tip radius for a given composition is identical to the one explained previously, but using the appropriate values of  $q_i^*$  to produce the IS contours.

### Application of the theory to Fe-C-Mo

To illustrate the use of the theory, it has been applied to calculate the lengthening rate of Mo<sub>2</sub>C needle-shaped precipitates growing in a ferrite matrix in a Fe-0.11C-1.95Mo alloy. Measurements on the lengthening rates and needle tip radius have been performed by Hall *et al.* [14] for a number of temperatures, and their data are shown in Table 1.

$T$ [K]	873	923	973	1023
measured $\rho$ [Å]	25	30	35	40
measured $v$ [ $\times 10^{-12}$ m s <sup>-1</sup> ]	1.0	10	130	220
$D_2/D_1 \times 10^6$	23	9.5	4.3	2.1
$\Omega_{Mo}$	0.0165	0.0159	0.0150	0.0132
$\Omega_C$	0.0149	0.0145	0.0139	0.0130
$p_{Mo} \times 10^{-3}$	2.25	2.11	1.92	1.60
$\rho/\rho_c$	21.6	20.8	20.1	19.6
$\rho$	11	18	30	49
$v$ [ $\times 10^{-12}$ m s <sup>-1</sup> ]	2.0	6.8	18	40

Table 1: Mo<sub>2</sub>C tip radius and average Mo<sub>2</sub>C lengthening rates in Fe-0.11C-1.95Mo [14], and those obtained from the application of the theory.

The diffusion coefficients of C and Mo are calculated from

$$D = D_o \exp\left\{-\frac{Q}{RT}\right\} \quad (17)$$

where  $R = 8.314$  J mol<sup>-1</sup> K<sup>-1</sup> is the universal gas constant,  $T$  the absolute temperature. For molybdenum,  $D_o = 1.1 \times 10^{-4}$  m<sup>2</sup> s<sup>-1</sup> and  $Q = 240 \times 10^3$  J mol<sup>-1</sup> [15]. For carbon,  $D_o = 2.2 \times 10^{-4}$  m<sup>2</sup> s<sup>-1</sup> and  $Q = 122 \times 10^3$  J mol<sup>-1</sup> [16].

The critical radius was obtained from equation (12) with  $\sigma = 0.2471$  J m<sup>-2</sup> [17],  $v_C^\beta$  and  $v_{Mo}^\beta$  were approximated as  $1.25 \times 10^{-29}$  m<sup>3</sup> atom<sup>-1</sup>; and  $c_i^{\alpha\beta}$  and  $c_i^{\beta\alpha}$  were obtained from a tie-line satisfying equation (13), which was provided by a thermodynamical database and phase diagram software MTDATA [18].

The values of  $D_2/D_1$  were found to be  $\sim 10^7$  (Table 1), and the IS contours corresponding to the values of  $\rho/\rho_c$  that intersect supersaturations  $\Omega_{Mo}$ ,  $\Omega_C$  were chosen. The tip radii and lengthening velocities associated to these calculations are shown in Table 1.

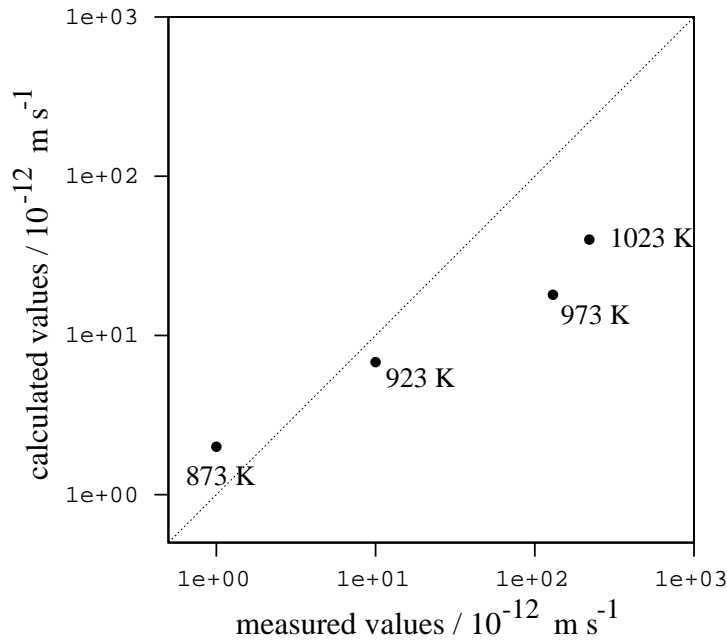


Fig. 8 Comparison between measured and calculated lengthening rates for the indicated temperatures

The measured and calculated lengthening velocities shown in Table 1 are presented graphically in Fig. 8, where it is seen that reasonable agreement is obtained.

### Summary

Consistent with Trivedi's work on the growth of needle shaped particles for binary systems, the incorporation of capillarity into the corresponding model for multicomponent systems introduces a minimum value of the supersaturation  $\Omega$  under which growth will not occur.

The diffusion-controlled growth rate tends to infinity as  $\Omega \rightarrow 1$ . This is not expected in practice because other rate-controlling processes become limiting at high needle lengthening-rates. Therefore, finite growth rates are obtained as  $\Omega \rightarrow 1$  when interfacial kinetic effects are introduced into the model. This again is consistent with Trivedi's work. However, with multicomponent systems, it becomes possible to obtain a unique solution for the velocity, without invoking a maximum velocity hypothesis. This method was applied to obtain lengthening rates of  $\text{Mo}_2\text{C}$  and their tip radius, obtaining reasonable agreement with experimental observations.

## Acknowledgements

The authors are grateful to the Mexican National Council of Science and Technology (CONACYT) and the Cambridge Overseas Trust for financial support, and Prof. A. Windle for providing laboratory facilities. One of the authors (PEJRDC) is grateful to the Committee of Vice-Chancellors and Principals of the Universities of the United Kingdom for the Overseas Research Studentship.

## References

1. Ivanstov, G. P. : *Dokl. Akad. Nauk, SSSR* **58** (1947) 567-569
2. Horvay, G., Cahn, J. W. : *Acta Metallurgica* **9** (1961) 695-705
3. Abramowitz, M. : *Handbook of Mathematical Functions*, (1965) New York, John Wiley
4. Trivedi, R. : *Acta Metallurgica* **18** (1970) 287-296
5. Trivedi, R. : *Acta Metallurgica* **1** (1970) 921-927
6. Christian, J. W. : *Theory of Transformations in Metals and Alloys*, 2nd edn, Part I (1975) Oxford, Pergamon Press
7. Rivera, P.E.J., Bhadeshia, H.K.D.H., *Materials Science and Technology* **17** (2001) 25-29
8. Zener, C. : *Trans AIME*, **167** (1946) 550-595
9. Bhadeshia, H. K. D. H. : *Materials Science and Technology*, **1** (1985) 497-504
10. Bhadeshia, H.K.D.H. : *Progress in Material Science*, **29** (1985) 321-386
11. Coates, D.E. : *Metallurgical Transactions*, **3** (1972) 1203-1212
12. Coates, D.E. : *Metallurgical Transactions*, **4** (1973) 2313-2325
13. Coates, D.E. : *Metallurgical Transactions*, **4** (1973) 1077-1086
14. Hall, M. G., Kinsman, K. R. and Aaronson, H. I. : *Metall. Trans* (1972) **3**, 1320-1322
15. Friedberg, J., Törndahl, L. and Hillert, M. : *Jerkontorets Ann.*, 1969, **1953**, 263-276
16. Wildinson, D. S. : *Mass Transport in Solids and Fluids* (2000) Cambridge University Press
17. Fujita, N. and Bhadeshia, H.K.D.H. : *Mater. Sci. and Technol.*, **15** (1999) 627-634
18. "MTDATA: Metallurgical and thermochemical databank", National Physical Laboratory, Teddington, Middx, UK, 1995.

## Appendix A

In Fig. 4 the lines for  $D_2/D_1 = 1$  terminate in limiting (forbidden) supersaturations; these depend on the value of  $\rho/\rho_c$  as shown in Fig. 3. The minima can be obtained when equation (9) is expressed as

$$\Omega_i = \frac{g^*\{p_i\}}{1 - \frac{\rho}{\rho_c} g^*\{p_i\} R_2\{p_i\}} \quad A1$$

and setting

$$\frac{d}{dp_i} \left\{ \frac{g^*\{p_i\}}{1 - \frac{\rho}{\rho_c} g^*\{p_i\} R_2\{p_i\}} \right\} = 0 \quad A2$$

The solution of equation (A2) for  $p_i$  can be inserted in (A1) to obtain the variation of the minimum values of  $\Omega_i$  with  $\rho/\rho_c$ , as shown in Fig. A1.

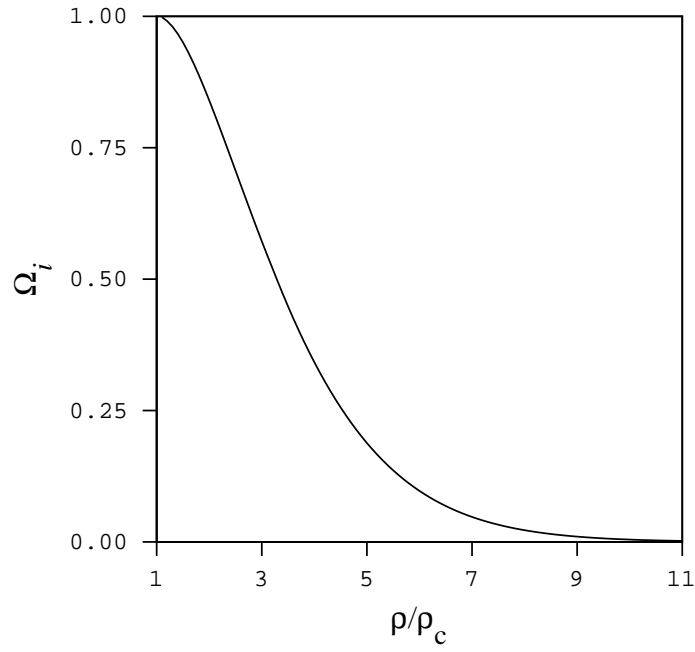


Fig. A1 Minimum values of  $\Omega_i$  as a function of  $\rho/\rho_c$